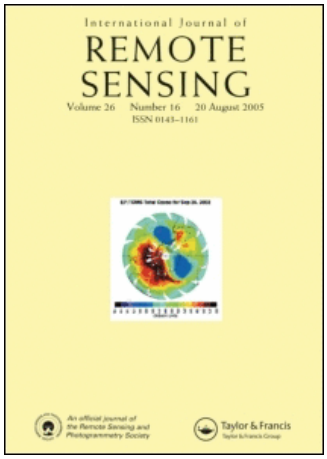

International Journal of Remote Sensing
Publication details, including instructions for authors and subscription information:
http://www.informaworld.com/smpp/title~content=t713722504

Characterizing the surface heterogeneity of fire effects using multi-temporal reflective wavelength data

D. P. Roy [a]; T. Landmann [b]
[a] Department of Geography, College Park, and NASA Goddard, Space Flight Center, University of Maryland. Code 614.5 (B32), Greenbelt, MD 20771. USA
[b] CSIR Environmentek. P.O. Box 395, Pretoria. South Africa

To link to this article: DOI: 10.1080/01431160500112783
URL: http://dx.doi.org/10.1080/01431160500112783

International Journal of Remote Sensing
Vol. 26, No. 19, 10 October 2005, 4197–4218

Characterizing the surface heterogeneity of fire effects using multi-temporal reflective wavelength data

D. P. ROY*† and T. LANDMANN‡
†Department of Geography, University of Maryland, College Park, and NASA Goddard, Space Flight Center, Code 614.5 (B32), Greenbelt, MD 20771, USA
‡CSIR Environmentek, P.O. Box 395, Pretoria, South Africa

The relationship between changes observed in multi-temporal remotely sensed data and disturbance processes are increasingly being studied in support of various land process modelling and management decision applications. The possibility of mapping both the location and degree of change and retrieving information concerning the disturbance process are primary goals. This paper studies changes in reflective wavelength data caused by the action of fire. We consider the heterogeneity of fire effects in terms of the fraction of the observation that burned (f) and the combustion completeness (cc). A spectral mixture model and field and satellite observations of prescribed fires are used to examine the relationship between change in reflectance, and cc and f. The prescribed fires were lit in different South African savannah types during the SAFARI 2000 dry season campaign. Implications for the development of methods to retrieve cc and f, and for the development of methods to map the spatial extent of fire-affected areas with known detection capabilities are discussed.

1. Introduction

Satellite remote sensing provides the only practical means of monitoring biomass burning over large areas. In the last decade, various methodologies have been proposed to map the spatial extent of biomass burning using remotely sensed data (e.g. Kasischke and French 1995, Eva and Lambin 1998a, Barbosa *et al.* 1999, Fraser *et al.* 2000, Roy *et al.* 2002). Although these methods have provided useful information, their detection capabilities remain unclear, particularly with respect to the heterogeneity of the fire-affected area. To first order, the heterogeneity of fire-affected areas may be considered in terms of the spatial distribution of the burned components and the combustion completeness. The combustion completeness is a commonly used term and is defined as the fraction of fuel exposed to the fire which actually burns (Scholes *et al.* 1996, Shea *et al.* 1996). These parameters are important for understanding the effect of fire on vegetation structure and ecosystem processes (Knapp and Seastedt 1986, Trollope and Tainton 1986). They are important for estimating the amount of biomass burned and so for estimating trace gas and particulate emissions required to understand release of carbon and greenhouse gasses to the atmosphere (Levine 1996).

*Corresponding author. Email: droy@kratmos.gsfc.nasa.gov

International Journal of Remote Sensing
ISSN 0143-1161 print/ISSN 1366-5901 online © 2005 Taylor & Francis
http://www.tandf.co.uk/journals
DOI: 10.1080/01431160500112783

The combustion completeness and the spatial distribution of the burned components may vary as a function of surface property variations, including vegetation composition, structure and soil background, and the fire behaviour. Fire deposits charcoal and ash, removes vegetation, and alters the vegetation structure. The fire behaviour controls the severity of fire effects including the degree and parts of the vegetation structure that are burned (ground cover, canopy cover, woody components, etc.) and the reflectance of deposited charcoal and ash. Factors including the micrometeorological conditions (wind velocity, relative humidity, etc.) and the fuel type, mass, compaction, and moisture may influence the fire behaviour, the combustion completeness, and the burned–unburned patchiness (Stocks *et al.* 1996, Ward *et al.* 1996). Soil, rock surfaces and green or wet vegetation may not burn at any scale. Temporally, the remotely sensed signature of fire-affected areas may change depending on the degree of vegetation regrowth/recovery and the degree of charcoal and ash dissipation by the elements (Langaas 1995, Trigg and Flasse 2000).

Despite the different factors that determine the remotely sensed signature of fire-affected areas, methodologies to map their spatial extent have been developed for a number of remote sensing systems. Algorithms that use multi-temporal satellite data to take advantage of the temporal persistency of fire effects have received considerable attention for regional to continental scale mapping (e.g. Barbosa *et al*. 1999, Fraser *et al*. 2000, Roy *et al.* 2002). These methodologies have relied on classification or thresholding techniques to label remotely sensed observations as burned or unburned. In general, the accuracy of the data products produced by these algorithms has been inferred in a validation context by statistical comparison with independently collected data. No algorithm, or validation results, has been presented quantifying the expected detection capabilities with respect to the completeness of combustion or the spatial burn heterogeneity within the sensed observations. This may be due to the empirical nature of the algorithms and difficulties in collecting sufficiently representative independent data. However, this poses a potential limitation on the appropriate use of these data. No methodology to map combustion completeness using remote sensing has been demonstrated, although multi-temporal high spatial resolution satellite data have been used to map ordinal classes of parameters that are related to combustion completeness, such as fire severity (e.g. Michalek *et al*. 2000, Rogan and Yool 2001, Miller and Yool 2002).

This paper examines the relationship between the change in reflectance caused by the action of fire and the heterogeneity of fire effects. A simple reflectance model parameterized for the combustion completeness (cc) and the fraction of the remotely sensed observation that burned (f) is used to investigate the influence of these parameters. We compare changes in Landsat reflectance with cc and f derived from field measurements at prescribed fires lit in South Africa to substantiate and illustrate the model findings. We discuss the implications of our findings for algorithms that examine change in reflectance to map fire-affected areas and discuss the possibility of deriving cc and f from multi-temporal reflectance data.

2. Modelling

The ability to differentiate between burned and unburned remotely sensed observations depends on the spatial distribution and spectral contrast of the burned and unburned components sensed in each observation and on the sensor's geometric

and radiometric characteristics (Eva and Lambin 1998b). To examine this in more detail, a modelling approach is used so that: (1) a range of model parameter values may be investigated that would be difficult to define using satellite data; (2) we avoid the need to normalize uncertainties, caused for example by changing sensing and surface conditions; (3) the model may be used in a predictive capacity.

In this paper, we only model optical remote sensing at reflective wavelengths, noting, however, that remotely sensed temperature estimates and thermal wavelengths have been used to aid differentiation between burned and unburned vegetation (e.g. Cahoon *et al.* 1994, Eva and Lambin 1998a, Barbosa *et al.* 1999). The noise free optical imaging process may be modelled as the convolution of the scene radiance with the sensor point spread function (PSF). Usually the sensor optics, detector, electronic filters, and sensor motion are modelled as a single acquisition PSF by convolving the individual PSFs of these effects together (Reichenbach *et al.* 1995). The optical image collected at the sensor is digitized and quantized into discrete values for electronic storage and transmission. The measurement made by a detector will be referred to as an observation, and the sensed surface dimensions will be referred to as the observation area. Assuming that observations are cloudless, uncontaminated by atmospheric effects, and that there is no significant amount of multiple scattering between the different scene components, then the sensed reflectance can be modelled as equation (1). This is the linear mixture model (Settle and Campbell 1998). In this model, the reflectance contributions of the scene components sensed in an observation are directly proportional to their surface areas.

$$\begin{aligned} \mathbf{x} &= \mathbf{M}\mathbf{p} + \mathbf{e} \\ \sum p_c &= 1 \text{ and } p_c \geq 0 \text{ for all } c, \end{aligned} \tag{1}$$

where $\mathbf{x}$ is an $(n \times 1)$ matrix describing the observed multi-spectral signal for n wavelengths, $\mathbf{p}$ is a $(c \times 1)$ matrix describing the ground cover proportions of c scene components, $\mathbf{M}$ is a $(n \times c)$ matrix whose columns describe the scene component endmember spectra, i.e. the response received in the absence of noise by an observation composed only of a single scene component, and $\mathbf{e}$ is an $(n \times 1)$ matrix describing the noise.

We model the effect of fire using two parameters, the combustion completeness and the fraction of the observation area that burns. The combustion completeness is defined in equation (2) as the ratio between the fire fuels consumed and the pre-fire fuel (Scholes *et al.* 1996, Shea *et al.* 1996).

$$\begin{aligned} cc &= (b_{t1} - b_{t2})/b_{t1} \\ 0 &\leq cc \leq 1, \end{aligned} \tag{2}$$

where cc is the combustion completeness, b_{t1} and b_{t2} are the pre-fire and post-fire fuel loads ($\mathrm{g\,m^{-2}}$) (based on dry matter weight) respectively. We consider the fraction of the observation area that burns in a spatial two-dimensional sense, ignoring the vertical dimension and recognizing that dense tree canopies with high leaf area index may obscure the understory signal (Fuller *et al.* 1997) and so obscure understory burns (Thompson 1993).

We model the simple case where the same proportions of the different scene components burn and where the completely burned scene components ($cc=1$) have the same endmember spectra. We assume that the relative proportions of

background soil and shade are the same before and after the fire. We assume no noise. In this case, the observed burned reflectance for a given wavelength, assuming linear mixing in equation (1), is modelled as equation (3).

$$x = (1-f)\rho_u + f(1-cc)\rho_u + cc\, f\, \rho_b \quad 0 \le f \le 1 \text{ and } 0 \le cc \le 1, \tag{3}$$

where x is the observed reflectance, cc is the combustion completeness, f is the fraction of the observation area that burned, ρ_u and ρ_b are the unburned and completely burned ($cc=1$) endmembers, respectively (i.e. the reflectances measured if the observation area contained only the unburned and completely burned material, respectively).

3. Study area and prescribed fires

Prescribed surface fires were lit in South Africa during the SAFARI-2000 dry season campaign (Swap *et al.* 2002) in the Kruger National Park (KNP), located along the Mozambican border, and in the Madikwe Game Reserve (MGR) (approximately 900 km west of the KNP). Both the KNP and the MGR are within savannah ecosystems where the soil properties, precipitation, and plant and animal competition regulate the biomass available for burning. In South Africa, most burning occurs in the dry season, from approximately June to October, when the vegetation fuel (litter, grass, fine leaves and branches) is senescent. The prescribed fires were primarily head fires started from line ignitions aligned along the perimeters of demarked areas and along road and seepage lines. The results from 19 fires (12 in KNP and seven in MGR) are presented in this paper.

The KNP is characterized by predominantly weathered granite derived soils with coarse and fine sandy loam, undulating topography (slope between 2 and 5°), and precipitation ranging from 500 mm to 900 mm per annum (Kruger *et al.* 2002). Experimental plots have been purposefully burned in the KNP every 1–3 years since 1954 (Biggs and Potgieter 1999). We examined prescribed fires lit on experimental plots near Pretoriuskop, in the south-west of the park, and near Satara, in the centre of the park. The Pretoriuskop plots are in parkland Sourveld savannah (Gertenbach 1983) with dominant *Combretum collinum*/*C zeyheri, Terminalia sericea* tree species, Sicklebush (*Dichrostachys cineria*) and *Acacia* shrub species, and tall growing *Hyperthelia dissoluta* grasses (Trollope and Potgieter 1986, Shea *et al.* 1996). The plots near Satara are in less wooded Marula Knobthorn savannah (Gertenbach 1983) with *Sclerocarya caffra* (Marula) and *Acacia* tree species and shorter growing grasses such as *Aristida* (Trollope and Potgieter 1986). All of the KNP plots had relatively small amounts of exposed soil (less than approximately 5% by surface area). The prescribed fires consumed the majority of the litter and much of the grass, shrub and tree canopy material below approximately 2 m. Trees taller than 2 m were moderately scorched. Some large fallen wood litter (diameter >1.5 cm) was left unburned at the Pretoriuskop plots. Prior to the fires, the vegetation in the different Pretoriuskop plots was observed to be approximately 30–60% green and in the Satara plots approximately 10–15% green.

The MGR is composed of savannah parklands (Thorn Bushveld) (Cole 1986) with *Boscia* tree species and dominantly *Arcacia* shrub species and a mix of tall grass species such as *Hyperthelia* as well as short *Aristida* and *Eragrostis* grass species (Scholes 1997). Soils are derived from weathered granite with black turfs and sandy

loams, and precipitation ranges from 400 mm to 500 mm per annum (Schulze 1997). Prescribed fires lit on relatively flat valley plains (slope $<4^{\circ}$) to counteract bush encroachment were examined. As at KNP, the MGR prescribed fires consumed the majority of the litter and most of the standing grass. There were slightly more exposed soil surfaces (approximately 5–10% surface area), less standing grass, and a higher shrub density than at the KNP. More shrub material was combusted than at the KNP resulting in spatially more patchy burns. Soil colour variability was higher at the MGR than at the KNP. Prior to the fires, the MGR vegetation was more senescent than at the KNP and was observed to be approximately 5–15% green.

4. Satellite data

Landsat ETM+ data were acquired for quantitative comparison with the field data collected in the KNP and the MGR. Radiometrically and geometrically corrected (Level-1G) Landsat ETM+ data acquired shortly before and after the prescribed fires at KNP and MGR were obtained (table 1). The Landsat data were acquired within 8 days of the different prescribed fires, except the pre-fire KNP Pretoriuskop Landsat data, which were acquired 2 months before the fires due to persistent cloud cover.

The Landsat ETM+ data were converted from digital counts to at-sensor radiance using Landsat calibration coefficients and then converted to at-sensor reflectance. In this study, only the Landsat 30 m reflective bands were considered. The shorter-wavelength Landsat bands were strongly contaminated by smoke aerosols because of the large amount of biomass burning in the region. Consequently, the at-sensor reflectance data were atmospherically corrected to surface reflectance using the 6S radiative transfer code (Vermote *et al.* 1997). The 6S

Table 1. Dates of prescribed fires lit at the Madikwe Game Reserve and Kruger National Park, Landsat ETM+ data characteristics, and AERONET aerosol optical thickness (AOT), water volume and air mass measurements made at Skukuza, Kruger National Park.

	Madikwe Game Reserve		Kruger National Park		
Date of prescribed fire 2000	18 August and 20 August (seven fires)		14 August (six Pretoriuskop fires) 22 August (six Satara fires)		
ETM acquisition date 2000	11 August	27 August	12 June	15 August	31 August
ETM path/row	172/077	172/077	168/077	168/077	168/077
ETM sun elevation angle (°)	38.1	42.6	32.7	39.2	43.9
ETM cloud cover (%)	0	0	34	49	0
ETM overpass time (GMT)	8:05	8:05	7:40	7:40	7:40
AERONET time (GMT)	8:06	8:03	6:55 and 12:55	8:29	7:40
AOT 1020 nm	0.08	0.11	0.12*	0.03	0.13
AOT 870 nm	0.10	0.15	0.13*	0.03	0.17
AOT 670 nm	0.16	0.23	0.20*	0.04	0.27
AOT 500 nm	0.27	0.37	0.35*	0.05	0.45
AOT 440 nm	0.33	0.43	0.42*	0.05	0.54
AOT 380 nm	0.42	0.54	0.54*	0.08	0.68
AOT 340 nm	0.50	0.61	0.62*	0.09	0.78
Water (cm)	2.08	2.70	2.77*	2.09	1.57
Air mass (unitless)	1.51	1.40	2.34*	1.40	1.46

*AERONET data linearly interpolated from 12 June measurements made 6:55 GMT and 12:55 GMT to 7:40 GMT.

code was run using Aerosol Robotic Network (AERONET) (Holben *et al.* 1998) aerosol optical depth, water volume and air mass measurements, summarized in table 1, and assuming KNP and MGR elevations of 400 m and 900 m, respectively. The AERONET data were measured at Skukuza, in the KNP, on the same dates and at approximately the same times as the Landsat overpasses. Although the geolocation accuracy of the Landsat data was high, it was necessary to coregister several dates to improve their coregistration to less than one 30 m Landsat pixel. This was achieved by inspecting ground control points and then translating the data by an integer number of pixels.

5. Field measurements

Field measurements were made at different sites located within areas burned by the MGR and KNP prescribed fires. The field measurements were used to estimate the site-level combustion completeness and the proportion of the site area that burned. In addition, samples of ash and non-photosynthetic vegetation fuel were collected for spectral analysis. Combustion completeness was calculated from equation (2) as the proportion of the total pre-fire fuel load (standing grass, standing woody vegetation, and litter) that burned. Estimates of the proportion of the site area that burned were made as part of the field sampling. A 120 m × 120 m site dimension was used, as it afforded a manageable size for field measurement, while allowing a large number of different sites to be examined, and was sufficiently large to minimize potential problems with Landsat ETM+ navigation.

Sites that were judged from extensive pre-fire field inspection and examination of the Landsat ETM+ data to have homogenous vegetation structure and composition, and to have relatively low amounts of tree cover (less than approximately 50%), were considered. Data collected during the prescribed burning, including type of fire (head or back fire), length of the flaming front and fire climate parameters (relative humidity and wind velocity), are not reported here but were used in conjunction with visual observations to reject inadequately burned sites. Only sites that were judged to have all their litter biomass completely burned were considered. It is recognized that some sites may have contained residual uncombusted litter biomass, but in general all surface fine fuels were removed by fire. Shea *et al.* (1996) noted that 96% of all litter is typically combusted by surface fires in the KNP. Only sites that were judged to have burned uniformly with the same combustion completeness were considered. Variations in the site conditions and the fire behaviour reduced the total number of sites that met these criteria. The results from 19 sites (12 KNP and seven MGR) are presented in this paper.

5.1 *Pre-fire field measurements*

At each 120 m × 120 m site, the standing grass fuel load was estimated in two steps. A disc pasture meter, developed by Bransby and Tainton (1977), was used to measure the settling height of the standing grass every 6 m along transects spaced 30 m apart. Second, standing grass was clipped in 50 cm square quadrats located every 30 m along the same transects. The clippings were dried and weighed and used to calibrate the disc pasture meter using a transformed linear regression relating the disc meter settling height (cm) to the grass biomass (g) (Trollope and Potgieter 1986). The grass fuel load ($g\,m^{-2}$) was estimated using the regression equation for the site. Litter material (leaf and woody material such as dead wood and twigs less

than 1.5 cm in diameter) was collected within the same 50 cm quadrats. The litter material was subsequently, dried and weighed, and used to estimate the site litter fuel load ($g\,m^{-2}$).

The standing woody vegetation (i.e. trees and shrubs) could not be measured by destructive sampling. Consequently, the woody fuel load was estimated using published allometry equations applied to individual measurements of tree and shrub height (m), number of stems, and basal diameter (cm) in three $10\,m \times 10\,m$ plots located randomly across the site. The mean of the three plot estimates was taken as the site-level standing woody fuel load ($g\,m^{-2}$). Up to 21 allometry equations were used. It is recognized that uncertainties may be introduced by this approach depending on the measurement accuracy and the degree that the allometry equations were representative of the site's woody vegetation at the time of measurement. Allometry equations derived by sampling KNP vegetation in the dry season were used (Netshiluvhi and Scholes 2001). Estimates of the percent tree cover were made using a spherical densiometer (Lemmon 1957) every 6 m along transects spaced 30 m apart. The percent tree cover data were used to reject sites with high tree cover. The seven MGR selected sites had estimated percent tree cover ranging from 0% to 25% (mean 13%), and the 12 KNP sites had percent tree cover ranging from 5% to 50% (mean 20%).

5.2 *Post-fire measurements*

At each $120\,m \times 120\,m$ site, the post-fire grass fuel load was estimated using the disc pasture meter only in areas where the unburned and partially burned grasses were left standing. The litter fuel load was not measured (only sites judged from field inspection to have all their litter biomass completely burned were considered). The percentage of woody standing biomass left after the fire in the three $10\,m \times 10\,m$ plots was estimated visually. Visual estimates were made below the maximum flame scorch height (approximately 2.5 m). The post-fire woody fuel load ($g\,m^{-2}$) was derived by subtracting this percentage from the pre-fire estimate.

Estimates of the proportion of the site area that burned were made as part of the field sampling. The 50 cm square quadrats located every 30 m along transects spaced 30 m apart were examined. If a quadrat contained more than 50% unburned material, it was considered unburned. Quadrats were unburned because of heterogeneity of the vegetation fuel and fire behaviour, or because they contained bare soil. Ash samples were collected across each site after the prescribed fires had cooled. Fires of different temperatures are known to produce ash of different shades, with hot fires producing white ash and cool fires producing blacker ash (Stronach and McNaughton 1989). A total of 850 g (dry weight) of black and white ash samples were collected in the KNP and MGR sites for subsequent spectral analysis.

6. Reflectance spectra measurements and results

The reflectance spectra of the black and white ash samples and samples of non-photosynthetic vegetation fuel were measured using an Analytical Spectral Devices (ASD) radiometer. The non-photosynthetic vegetation fuel material was composed of equal parts of the pre-fire dried grass clippings and litter. The ASD measurements were taken in the laboratory to reduce field measurement errors and because we were concerned only with obtaining representative spectra for illustrative modelling.

The measurements were made under diffuse illumination conditions in the spectral range 350–2500 nm with the ASD radiometer aligned perpendicular to the samples to simulate nadir remote sensing conditions. We measured the KNP and MGR samples separately.

The measured spectra are shown in figure 1. Dry long grass spectra collected from the Pierre shale, Canon City, Colorado, provided by the USGS Digital Spectral Library (Clark *et al*. 1993), are also shown. The most obvious spectral change evident in figure 1 is the decrease in reflectance from unburned non-photosynthetic vegetation fuel to black ash over all but the shortest wavelengths of the 350–2500 nm region. The white ash samples have a higher reflectance than the black ash and are higher than both the non-photosynthetic vegetation fuel and the USGS dry long grass spectra. This illustrates an important issue. Fires that are sufficiently hot to produce white ash may not be detected using methods that expect a drop in reflectance associated with biomass burning. Similarly, methodologies to relate change in reflectance to fire properties, such as combustion completeness, may be biased significantly by the presence of white ash.

7. Illustrative modelling results

The non-photosynthetic vegetation fuel and black ash reflectance measurements illustrated in figure 1 were used as unburned and burned endmembers in equation (3) to model the relationship between observed reflectance, combustion completeness (cc), and the fraction of the observation area that burned (f). Figure 2 shows modelled reflectance values over the full range of cc and f using the average of the KNP and MGR non-photosynthetic vegetation and black ash ASD reflectance measurements at 1240 nm. The 1240 nm wavelength has been shown to provide good

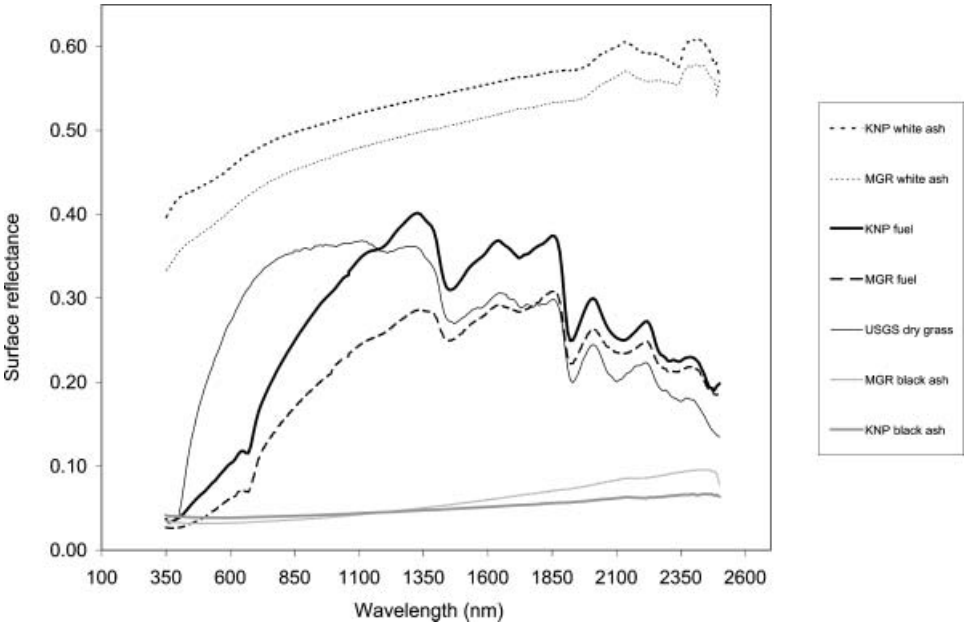

Figure 1. Reflectance spectra of black and white ash and non-photosynthetic vegetation fuel samples made using an ASD radiometer. The samples collected from the Kruger National Park (KNP) and the Madikwe Game Reserve (MGR), South Africa.

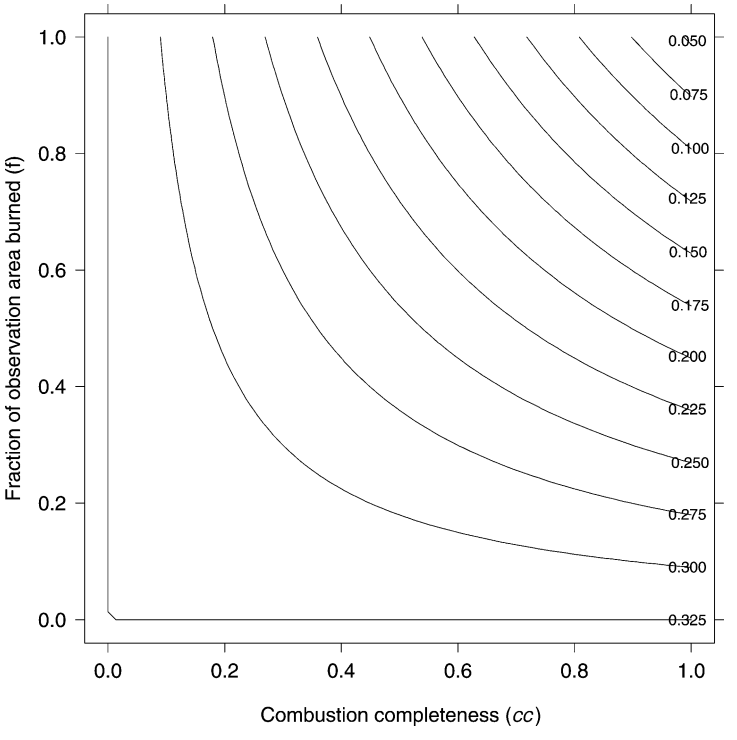

Figure 2. Modelled reflectances for a hypothetical observation sensed over a fire-affected area with different combustion completeness and fraction of the observation area that burned. Reflectances modelled using the average of the KNP and MGR non-photosynthetic vegetation and black ash 1240nm ASD reflectance measurements (ρ_u=0.325 and ρ_b=0.046).

burned–unburned discrimination in field measurements made in Namibia (Trigg and Flasse 2000), and by empirical examination of MODIS surface reflectance data over most of southern Africa (Roy *et al.* 2002). The reflectance decreases as either *f* or *cc* increases. The decrease in reflectance is linear as a function of either *cc* or *f* holding the other fixed. Figure 2 illustrates that there are an infinite number of *cc* and *f* combinations that may produce the same observed decrease in reflectance after a fire. This implies that methodologies that attempt to retrieve *cc* or *f* will not work reliably without knowledge of one of these parameters. This is illustrated using the Landsat ETM+ data and field measurements in the following section.

Spectral indices are used by many remote sensing applications and have been widely used to map the spatial extent of fire-affected areas. This is primarily because spectral indices have attractive properties, such as normalizing certain illumination and topographic variations, and because alternative more physically based approaches, for example, based upon inverting models against reflectance measurements are significantly less easy to implement (Verstraete and Pinty 1996, McDonald *et al.* 1998). Figure 3 shows modelled reflectance plotted as a function of *f* for fixed *cc* using average KNP and MGR non-photosynthetic vegetation and black ash ASD reflectance measurements at 1240 nm and 2130 nm. The 2130 nm wavelength is less sensitive to burning than 1240 nm (the reflectance gradient is smaller) which has been observed previously (Trigg and Flasse 2000, Roy *et al.* 2002). Figure 4 shows a spectral index computed as the difference between the

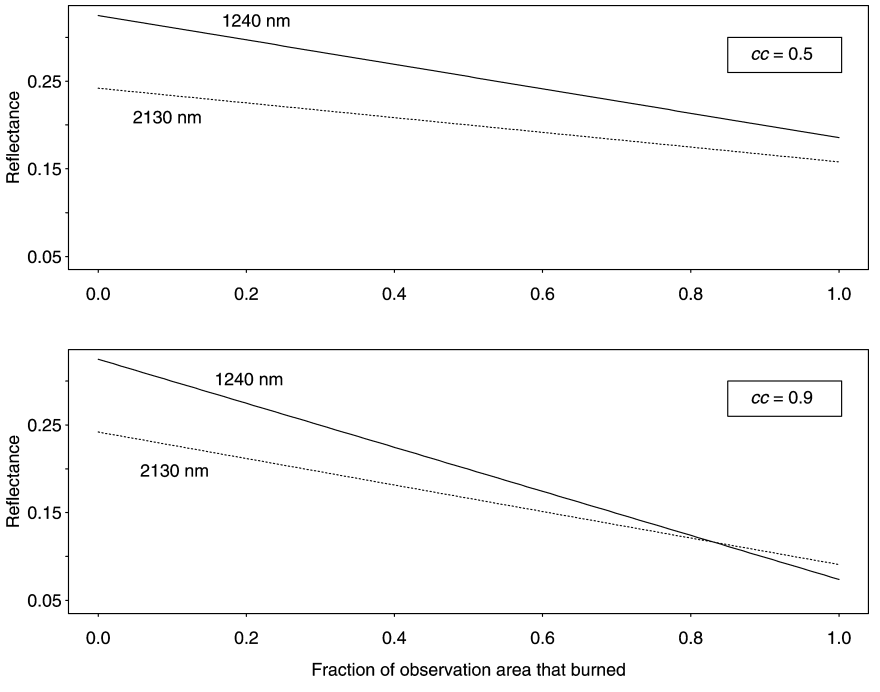

Figure 3. Modelled reflectances for a hypothetical observation sensed over a fire-affected area with combustion completeness=0.5 (top) and combustion completeness=0.9 (bottom) plotted as a function of the fraction of the observation area that burned. Reflectances modelled at 1240nm (solid line) and 2130nm (dashed line) using the average of the KNP and MGR non-photosynthetic vegetation and black ash ASD reflectance measurements at these wavelengths (1240nm: ρ_u=0.325 and ρ_b=0.046; 2130nm: ρ_u=0.242 and ρ_b=0.074).

2130 nm and 1240 nm reflectance divided by their sum. This ratio spectral index is illustrated because it appears to provide good burned–unburned discrimination using MODIS data. We note that similar indices have been found to provide good burned–unburned discrimination using Landsat TM band 4 (760–900 nm) and band 7 (2080–2350 nm) (Lopez Garcia and Caselles 1991), and using AVHRR band 1 (580–680 nm) and the reflective component of the middle-infrared AVHRR band 3 (3550–3930 nm) (Pereira 1999, Roy *et al.* 1999). The spectral index values were computed using the reflectance data illustrated in figure 3. Unlike the reflectance data, the spectral index values decrease in a nonlinear manner with respect to f (or to cc). This implies that ratio-type spectral indices may be sensitive in a nonlinear manner to the size and combustion completeness of the fire. Consequently, they may provide variable detection capabilities when used to map fire-affected areas or to extract fire properties.

In biomass burning mapping approaches, the definition of the magnitude of spectral change associated with the conversion of vegetation to burned vegetation is critical. Figure 5 illustrates the change in reflectance for two fires modelled using different products of f and cc, illustrating a small and/or incomplete burn ($f \times cc$=0.25) and a larger and/or more complete burn ($f \times cc$=0.5). The change in reflectance is plotted as a function of the pre-fire reflectance to simulate different types of surface. Thresholds based on relative rather than absolute changes have been suggested as being useful to account for variability of spectral values due to

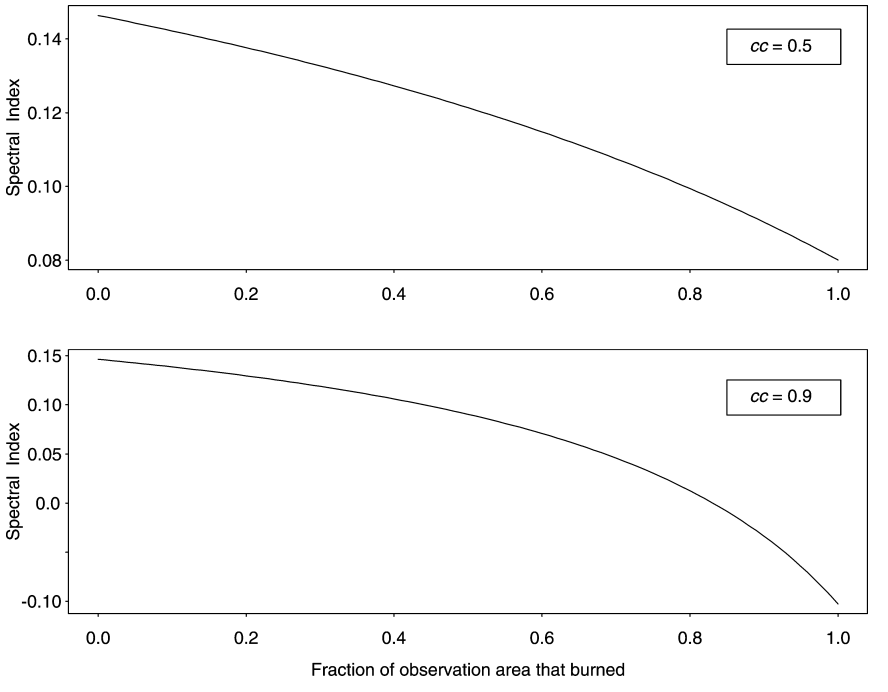

Figure 4. Modelled spectral index values for a hypothetical observation sensed over a fire-affected area with combustion completeness=0.5 (top) and combustion completeness=0.9 (bottom) plotted as a function of the fraction of the observation area that burned. Spectral index values computed as (ρ1240nm − ρ2130nm)/(ρ1240nm + ρ2130nm) using the reflectance data illustrated in figure 3.

biome type, soil characteristics etc. (Eva and Lambin 1998b). Accordingly, both the absolute change in reflectance (figure 5(*a*)) and the relative change in reflectance (figure 5(*b*)) are shown (solid lines). These reflectance data were modelled using the average of the KNP and MGR black ash 1240 nm ASD reflectance measurements. Figure 5 illustrates that burns with the same *f* and *cc* product exhibit reflectance changes that depend on the pre-fire reflectance. Evidently, burns on highly reflective surfaces (e.g. dry senescent grass) are more likely to be detected than burns occurring on less reflective surfaces (e.g. certain dense forest covers), and larger/completer burns are more likely to be detected than small/incomplete burns. Similar observations were made by Eva and Lambin (1998b). For example, in figure 5(*a*) an absolute reflectance threshold set with a value more negative than −0.15 will fail to detect the small/incomplete burn and will only detect the larger/completer burn if the pre-fire reflectance is greater than 0.4. The relative change in reflectance shown in figure 5(*b*) is nonlinearly dependent on the pre-fire reflectance. This nonlinearity is most pronounced when the pre-fire reflectance is low, implying caution in the application of relative reflectance thresholds for detection of burning over dark (low reflectance) surfaces.

Remote sensing data are noisy, due to the sensing system optics and electronics, the effect of the atmosphere, and data processing. The impact of noise is illustrated by the dashed lines in figure 5 which show the $\pm 1\sigma$ (one standard deviation) error computed analytically from [3] using the standard propagation of variance formula (Cooper 1987) and assuming that the before and after fire reflectance values are

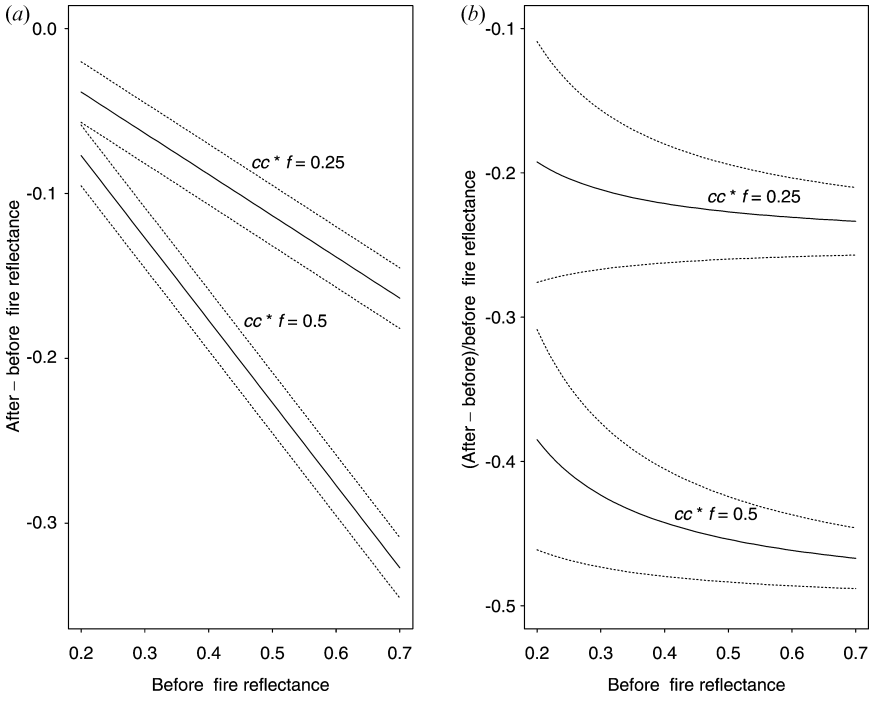

Figure 5. Modelled absolute (left) and relative (right) change in reflectance for a hypothetical observation sensed over of fire-effected areas with different combustion completeness (cc) and fractions of the observation area that burned (f), illustrating a small and/or incomplete fire ($f \times cc=0.25$) and a larger and/or more complete fire ($f \times cc=0.5$). Reflectances modelled using the average of the KNP and MGR non-photosynthetic vegetation and black ash 1240nm ASD reflectance measurements ($\rho_u=0.325$ and $\rho_b=0.046$). The dashed line shows modelled $\pm 1\sigma$ errors computed assuming normally distributed 1240nm reflectance errors with a mean value of zero and $1\sigma=0.013$. The modelled $\pm 1\sigma$ errors are constant (0.018) for absolute change in reflectance (a) and variable for relative change in reflectance (b).

independent. A reflectance error with a mean value of zero and $1\sigma=0.013$ is modelled corresponding approximately to the MODIS 1240 nm band land surface reflectance error inferred from preliminary validation of the MODIS land surface reflectance product (Vermote *et al.* 2002). The modelled error in the absolute change in reflectance is 0.018 (1σ) and is independent of the pre-fire reflectance (figure 5(a)). The modelled error in the relative change in reflectance decreases as the pre-fire reflectance increases (figure 5(b)). This reinforces the earlier observation concerning caution in the application of relative thresholds for detection of burning over dark surfaces. Noise imposes a lower limit on change detection capabilities. Figure 6 shows modelled absolute change in reflectance over the full range of cc and f using the MGR and KNP non-photosynthetic vegetation and black ash 1240 nm ASD reflectance measurements. Given the assumptions implicit to this modelling, then the illustrated cc and f values with absolute reflectance changes more negative than -0.018 are not expected to be detected reliably using MODIS 1240 nm land surface reflectance data. A modelled reflectance change of -0.018 occurs where the products of cc and f are 0.08 and 0.05 for MGR and KNP respectively (figure 6). This implies that burns with $cc \times f$ less than 0.08 and 0.05 will not be detected

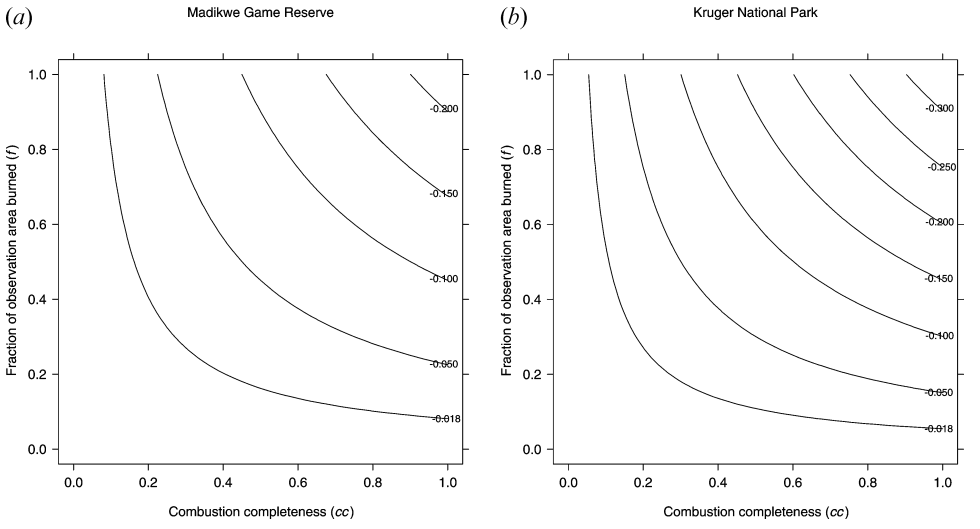

Figure 6. Modelled absolute change in reflectance (after and before fire reflectance) for a hypothetical observation sensed over a fire-affected area with different combustion completeness and fractions of the observation area that burned. Model results shown separately for (*a*) the MGR non-photosynthetic vegetation and black ash 1240nm ASD reflectance measurements (ρ_u=0.269 and ρ_b=0.047) and, (*b*) the KNP non-photosynthetic vegetation and black ash 1240nm ASD reflectance measurements (ρ_u=0.378 and ρ_b=0.046). The −0.018 reflectance change contour is equivalent to the modelled 1σ noise illustrated in figure 5(*a*).

reliably at the MGR and KNP sites, respectively. Larger and/or more complete burns will fail to be detected at the MGR site than at the KNP site because the spectral contrast between the non-photosynthetic vegetation and black ash samples collected at the MGR is smaller than at KNP. Clearly, other unmodelled factors will also impact detection capabilities. These include a reduction in spectral contrast since the time of fire, and changes in the relative proportions of background soil and shade before and after the fire.

8. Comparison of Landsat ETM+ reflectance and field measurements

Figure 7 illustrates the Landsat ETM+ surface reflectance data for the 12 KNP and 7 MGR sites before and after the prescribed fires. The Landsat data were acquired within 8 days of the prescribed fires, except at the six Pretoriuskop KNP fires (14 August) where 12 June and 15 August Landsat scenes were used (table 1). The mean cloud-free reflectance values for each 120 × 120 m site (derived from a maximum of 16 pixels) are shown. In general, burning reduces the mean surface reflectance, although for ETM+ bands 1, 2, 3 and 7, the differences between the mean unburned and burned reflectance values are small, which is expected from previous studies in African savannas (Landmann 1999). The pre-fire ETM+ band 4 (750–900 nm) KNP reflectance values are considerably higher than the MGR values because the KNP vegetation is less senescent (i.e. greener) with a smaller proportion of exposed soil surfaces. The ETM+ band 4 soil reflectance was approximately 0.3 at the KNP sites and varied from approximately 0.2 to 0.3 at the MGR sites (found by examination of visually identified soil pixels). Some of the KNP sites have a higher post-fire than pre-fire ETM+ band 1 (450–515 nm), reflectance which is probably due to

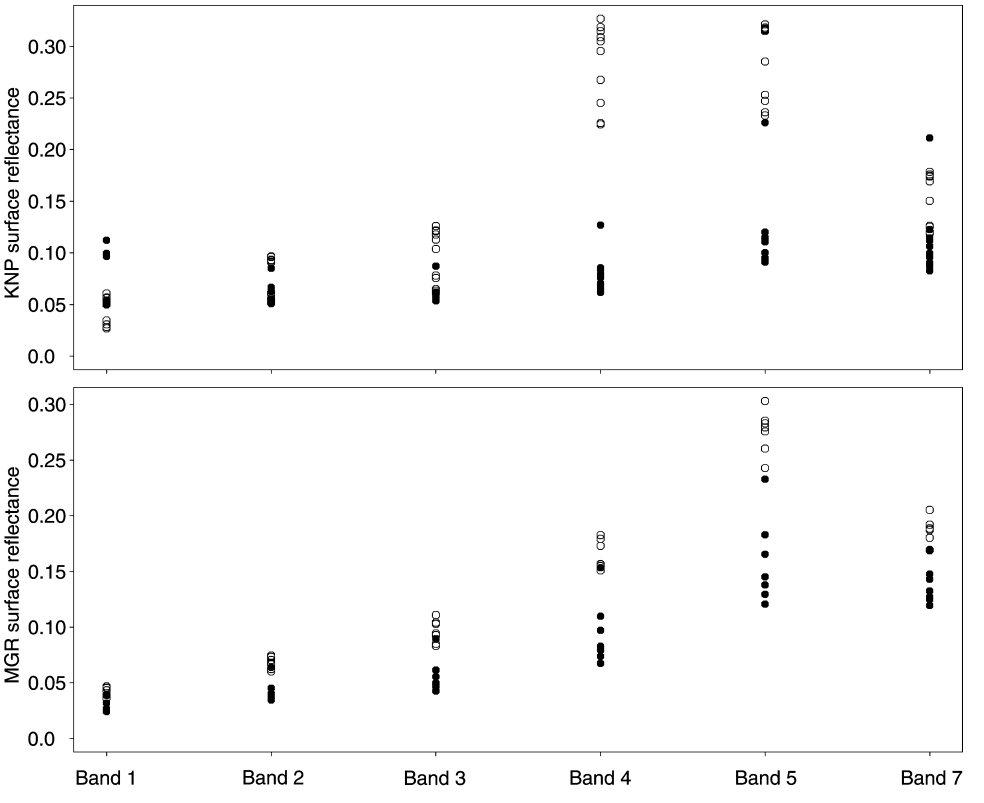

Figure 7. Landsat ETM+ surface reflectance data acquired before prescribed fires (open circles) and after prescribed fires (closed circles) at 12 sites in the Kruger National Park (KNP) (top) and at seven sites in the Madikwe Game Reserve (MGR) (bottom). The mean reflectance of the cloud-free 30m pixels falling within each 120m × 120m site are shown for Landsat bands 1 (450–515nm), 2 (525–605nm), 3 (630–690nm), 4 (750–900nm), 5 (1550–1750nm) and 7 (2090–2350nm).

inadequate aerosol correction of the shortest ETM+ wavelength band associated with the use of interpolated AERONET data (table 1). This may also be because the pre-fire reflectance for the six Pretoriuskop KNP sites was derived earlier in the dry season, under less senescent conditions, from a Landsat ETM+ scene acquired 2 months before the fire (table 1).

The field-based estimates of site-level combustion completeness (*cc*) and the proportion of the site area that burned (*f*) were compared with the satellite data to substantiate the modelling findings described in the previous section. Figures 8 and 9 illustrate comparisons of *cc* and *f* with the Landsat ETM+ band 4 data acquired before and after the prescribed fires. These figures show the absolute change in reflectance plotted as a function of *cc* and *f* for the different 30 m pixels (solid dots) at the 12 KNP and seven MGR sites. Regression fits of these data and the coefficient of determination (R^2) (used to indicate goodness of fit) are illustrated (solid lines). Regression fits of the mean of the 30 m ETM+ pixel values falling over each site are also shown (dashed lines) with R^2 values shown in the figure legends in parentheses. The regressions computed using the mean, rather than the original pixel values, produce similar fits but have inflated R^2 values and are significant at lower levels of confidence (which is expected from statistical theory). ETM+ band 4 results are

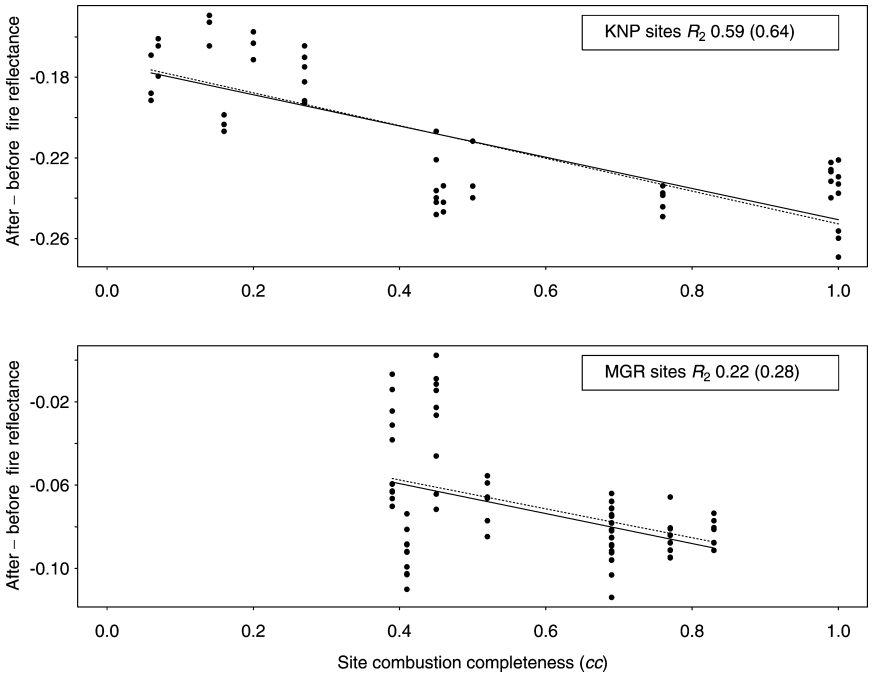

Figure 8. Change in Landsat ETM+ band 4 surface reflectance data acquired before and after prescribed fires at 12 sites in the Kruger National Park (KNP) (top) and at seven sites in the Madikwe Game Reserve (MGR) (bottom) plotted as a function of site-level estimates of combustion completeness. The change in reflectance for cloud-free 30m pixels falling within each 120m × 120m site (dots) with simple linear regression fits of these data (solid lines) and regression fits of the mean of the pixel values at each site (dashed lines, R^2 in parentheses) are shown.

illustrated because they consistently provided higher R^2 values than any other band, with similar results and only slightly lower R^2 values found using ETM+ band 5 (1550–1750 nm). The assumptions implicit to the regression analysis are probably not met here; in particular, the *f* and *cc* values cannot be assumed to have negligible error. Consequently, caution must be applied in the interpretation of these results.

The changes in ETM+ band 4 reflectance caused by burning are greater for the KNP than the MGR sites (figures 7–9). This is primarily because the pre-fire reflectance values are higher at KNP than MGR (figure 7) and not because the KNP sites have higher values of *cc* and *f* (figures 8 and 9). This underscores the observation made in the previous section that burns on highly reflective surfaces are more likely to be detected than burns occurring on less reflective surfaces. The variation in the change in reflectance at individual sites (figures 8–9) is no more than approximately 0.04 and 0.06 for the KNP and MGR sites, respectively. This variation may be due to noise in the ETM+ surface reflectance data and inadequate coregistration of the different dates. The variation may also be due to spatial differences in the pre-fire state and the homogeneity of fire effects across each site. For example, the variation may be greater at the MGR sites than at KNP because the MGR burns and underlying soil were spatially more heterogeneous. However, we note that the greatest variations occur for the two MGR sites that have the lowest *cc* and *f* values ($cc \times f < 0.2$, figure 10) and include pixels with small reflectance differences (less than 0.02 in magnitude). These reflectance differences

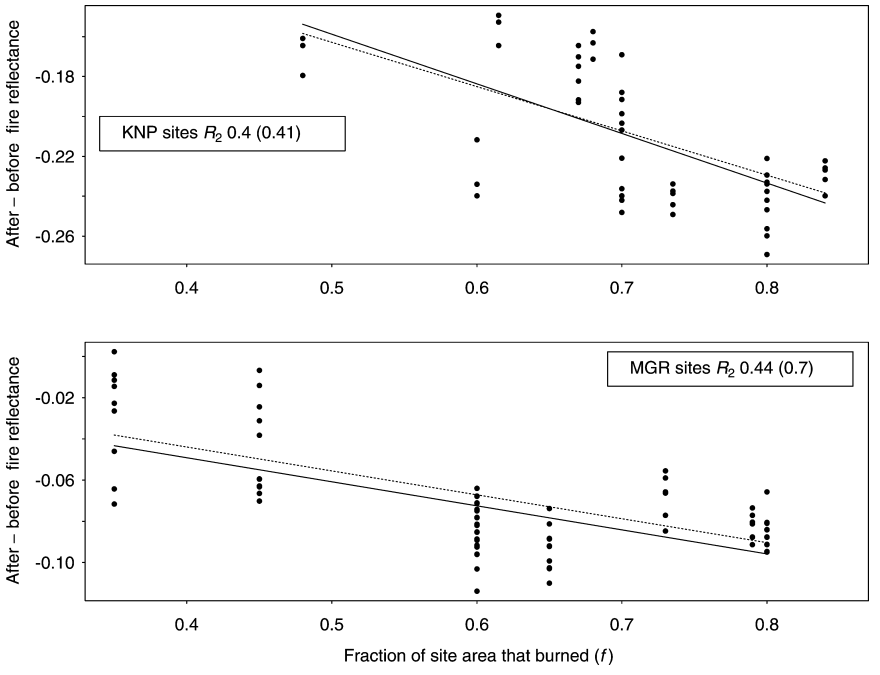

Figure 9. Change in Landsat ETM+ band 4 surface reflectance data acquired before and after prescribed fires at 12 sites in the Kruger National Park (KNP) (top) and at seven sites in the Madikwe Game Reserve (MGR) (bottom) plotted as a function of site-level estimates of the fraction of the site area that burned. The change in reflectance for cloud-free 30m pixels falling within each 120m × 120m site (dots) with simple linear regression fits of these data (solid lines) and regression fits of the mean of the pixel values at each site (dashed lines, R^2 in parentheses) are shown.

are sufficiently small that they may be close to the meaningful change detection limit when noise in the ETM+ surface reflectance data is taken into consideration. Small amounts of highly reflective white ash were observed at most of the sites after the prescribed fires (approximately 10% white to 90% black ash), but we have insufficient data to quantify the likely impact on the results presented here.

The modelling results presented in the previous section indicate that the change in reflectance after a fire is a linear function of f or cc holding the other parameter fixed, and that an infinity of cc and f combinations may produce a similar change (figures 2 and 6) in a manner dependent on the pre-fire reflectance (figure 5). Consequently, the linear regressions between the absolute change in Landsat ETM+ reflectance and the field measurements of cc and f, shown in figures 8 and 9, are not expected to describe the data perfectly. Despite this, the illustrated regressions are significant ($p<0.001$) and illustrate that cc and f independently explain variation in the change in reflectance due to burning. This supports the modelling results presented in the previous section that fires that burn a larger fraction of the observation or that have a higher combustion completeness produce a larger change in reflectance. At the KNP sites, R^2 values of 0.59 and 0.40 are found for cc and f, respectively. At the MGR sites, R^2 values of 0.22 and 0.44 are found for cc and f, respectively. The relationship between the change in reflectance and cc is stronger at KNP than at MGR. This may be related to the greater spectral contrast observed between the non-photosynthetic vegetation and black ash samples

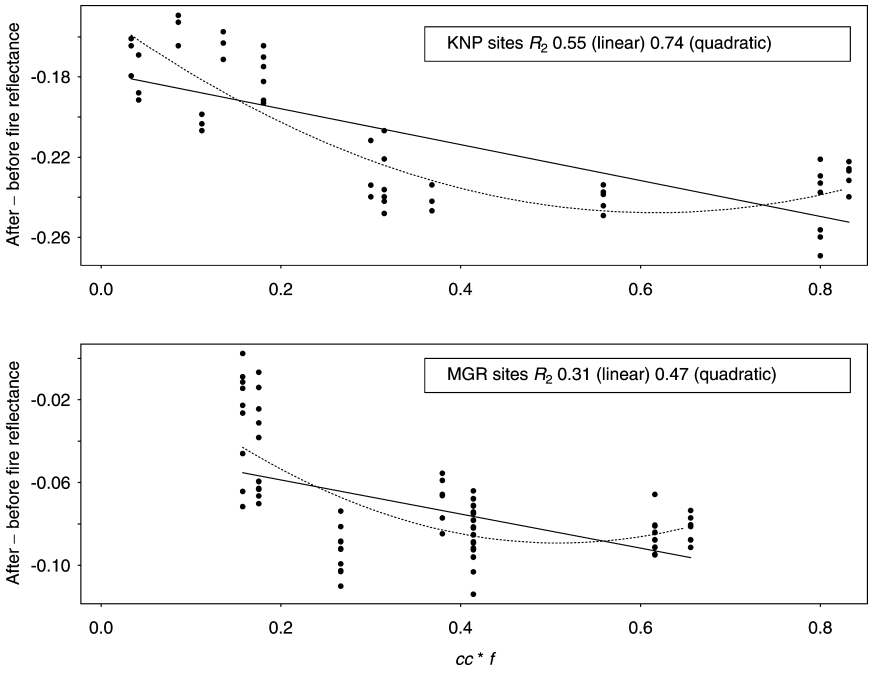

Figure 10. Change in Landsat ETM+ band 4 surface reflectance data acquired before and after prescribed fires at 12 sites in the Kruger National Park (KNP) (top) and at seven sites in the Madikwe Game Reserve (MGR) (bottom) plotted as a function of the product of estimates of the fraction of the site area that burned and the site-level combustion completeness. The change in reflectance for cloud-free 30m pixels falling within each 120m × 120m site (dots) with simple linear regression fits (straight lines) and quadratic regression fits (dashed curved lines) of these data are shown with R^2 in parentheses.

at KNP than MGR. However, this may also be due to sensitivity of the regression analysis to the relatively small range of *cc* values collected at the MGR sites (approximately 0.4–0.8) compared with the KNP sites (approximately 0.1–1.0) (figure 8). The MGR data, for the limited range of *cc* cases examined, have a stronger relationship between change in reflectance with *f* than with *cc* (figure 9). This may be indicative of the spatial soil heterogeneity in the pre-fire and post-fire reflectance observed at the MGR sites.

Multiple regression analysis using the absolute change in ETM+ reflectance as the dependent variable and both the *f* and *cc* field measurements as independent variables was not meaningful for the KNP and MGR data because of the limited distribution and number of field measurements (figures 8–9) relative to their underlying population (figure 6). The modelling results in the previous section indicate that the absolute change in reflectance is related to the product of *f* and *cc* in manner that is dependent on the pre-fire reflectance (figure 5(*a*)). Consequently, we examined the change in reflectance as a function of the product of *f* and *cc* (figure 10). Linear regression fits of these data gave R^2 values of 0.55 and 0.31 for the KNP and MGR data, respectively (figure 10). Quadratic regression fits gave improved R^2 values of 0.74 and 0.47 for the KNP and MGR data, respectively (figure 10). All the regressions illustrated in figure 10 are significant ($p<0.001$). As before, fires that have higher *cc* and *f* values produce a larger change in reflectance, although the quadratic regressions predict a decreased reflectance at the highest

$cc \times f$ values, which is not predicted by the modelling and again may be related to the limited distribution and number of field measurements. In general, although statistically significant, the regression relationships illustrated in figures 8–10 are not particularly strong. Evidently, if relationships of this nature were used in a predictive capacity, for example to predict *cc* and/or *f*, they would need to be applied in a site-specific manner.

9. Conclusions

The field and satellite observations and modelling results described in this paper demonstrate that both the combustion completeness (*cc*) and the fraction of the observation area that burns (*f*) influence the change in reflectance that occurs after the passage of fire. Consequently, methodologies that use change in reflectance to retrieve *f* or *cc*, or related fire properties, may not work reliably without prior knowledge of one of these two parameters. In addition, the results demonstrate that the change in reflectance observed for fires with the same product of *cc* and *f* will depend on the pre-fire reflectance. Further, the action of certain high-temperature fires is to deposit highly reflective white ash that may increase rather than decrease the reflectance after a fire (Stronach and McNaughton 1989), and so bias methodologies that expect a drop in reflectance associated with burning. As pre-fire reflectance, fire temperature, *cc* and *f* vary as a function of many factors, empirical relationships made between ground observations of these parameters and changes in reflectance may only be applicable in a local context, for example, for fire monitoring and management of protected areas (e.g. Biggs 2002) and local post-fire ecosystem rehabilitation studies (e.g. Miller and Yool 2002). Techniques used to classify satellite data into broadly defined fire severity classes (e.g. unburned, lightly burned, and severely burned) may be insensitive to these effects.

The findings described here imply that algorithms developed to make spatially explicit maps of fire-affected areas have variable detection capabilities. Algorithms may detect burns with different degrees of heterogeneity as the pre-fire reflectance changes (e.g. due to vegetation phenology), as the combustion completeness changes (e.g. due to the seasonally controlled amount of fuel moisture), and as the degree of spatial fragmentation of the burned surface changes. We recognize that detection variability may always be present, especially when classification approaches are used. However, this observation has implications for the utility of such data, and implies that their accuracy should be validated by examination of regions that include representative variations of *cc*, *f* and pre-fire reflectance.

The model presented in this paper is simple and is probably not representative of most fire-affected surfaces, such as, for example, certain forested ecosystems where spectral differences between burned and unburned vegetation are low, and the canopy structure introduces strong directional reflectance effects. The modelling results imply, however, that methods to map fire-affected areas may be less sensitive to noise, and provide less variable detection capabilities with respect to *f* and *cc*, by thresholding absolute changes in reflectance, rather than thresholding relative changes in reflectance, or thesholding ratio type spectral band indices such as that examined in this study. Finally, we note that the product of *f* and *cc* is related to the change in reflectance, and that this product multiplied with the fuel load ($g\,m^{-2}$) provides an estimate of the biomass burned (g) in a satellite observation. Retrieval of this information by remote sensing would provide a major advance over

anecdotal estimates of combustion completeness and assumptions that the entire satellite observation area burned that have been previously used for emissions estimation (e.g. Scholes *et al*. 1996, Barbosa *et al.* 1999). The use of well-calibrated, atmospherically corrected, cloud-screened, reflectance data, combined with less empirical mapping approaches, based for example upon inverting bi-directional reflectance models against surface reflectance measurements (Roy *et al*. 2002), may possibly allow the development of algorithms with known detection limits defined with respect to *f* and *cc* and the retrieval of the product of *f* and *cc*. Further work is required in these respects.

Acknowledgements

The authors thank Dr Robert Zomer of the International Centre for Research in Agroforestry (ICRAF), Nairobi, Kenya, for the ASD laboratory measurements. Tanja Kraus contributed greatly with the fieldwork and field data assessment, with additional field assistance provided by the Kruger National Park and Madikwe Game Reserve staff. We thank Dr Eric Vermote for his assistance with 6S and Dr Brent Holben for providing the Skukuza AERONET data. The Landsat project and EDC DAAC personnel are thanked for their assistance in securing ETM+ data with rapid turnaround. This research was supported by the Gottlieb Daimler and Karl Benz Foundation and the National Aeronautics and Space Administration (NASA) Land Use and Land Cover Change (LUCC) (grant NAG511251) program. This study was part of the SAFARI 2000 Southern African Regional Science Initiative.

References

BARBOSA, P.M., STROPPIANA, D., GRÉGOIRE, J-M. and PEREIRA, J.M.C., 1999, An assessment of vegetation fire in Africa (1981–1991): burned areas, burned biomass and atmospheric emissions. *Global Biogeochemical Cycles*, **13**, pp. 933–950.

BIGGS, H.C., 2002, *Proposed Policy for the Ecosystem Management of Fire in the Kruger National Park, Policy Revision Document* (Skukuza, South Africa: National Parks Board).

BIGGS, H.C. and POTGIETER, A.L.F., 1999, Overview of the fire management policy of the Kruger National Park. *Koedoe*, **42**, pp. 101–110.

BRANSBY, D.I. and TAINTON, N.M., 1977, The disc pasture meter: possible applications in grazing management. *Proceedings of the Grassland Society of Southern Africa*, **12**, pp. 115–118.

CAHOON, D.R., STOCKS, B.J., LEVINE, J.S., COFER, W.R. and PIERSON, J.M., 1994, Satellite analysis of the severe 1987 forest-fires in northern China and southeastern Siberia. *Journal of Geophysical Research*, **99**, pp. 18627–18638.

CLARK, R.N., SWAYZE, G.A., GALLAGHER, A.J., KING, T.V.V. and CALVIN, W.M., 1993, The US Geological Survey, Digital Spectral Library: Version 1: 0.2 to 3.0 microns. US Geological Survey Open File Report 93-592. Available online at: http://speclab.cr.usgs.gov (accessed 20 May 2003).

COLE, M.M., 1986, *The Savannas: Biogeography and Geobotany* (London: Academic Press).

COOPER, M.A.R., 1987, *Control Surveys in Civil Engineering* (London: Collins Professional Books), pp. 125–126.

EVA, H. and LAMBIN, E.F., 1998a, Burnt area mapping in Central Africa using ATSR data. *International Journal of Remote Sensing*, **19**, pp. 3473–3497.

EVA, H. and LAMBIN, E.F., 1998b, Remote sensing of biomass burning in tropical regions: Sampling issues and multisensor approach. *Remote Sensing of Environment*, **64**, pp. 292–315.

FRASER, R.H., LI, Z. and CIHLAR, J., 2000, Hotspot and NDVI differencing synergy (HANDS): A new technique for burned area mapping over boreal forest. *Remote Sensing of Environment*, **74**, pp. 362–376.

FULLER, D.O., PRINCE, S. and ASTLE, W.L., 1997, The influence of canopy strata on remotely sensed observations of savanna-woodlands. *International Journal of Remote Sensing*, **18**, pp. 2985–3009.

GERTENBACH, W.P.D., 1983, Landscapes of the Kruger National Park. *Koedoe*, **26**, pp. 9–121.

HOLBEN, B.N., ECK, T.F., SLUTSKER, I., TANRE, D., BUIS, J.P., SETZER, A., VERMOTE, E., REAGAN, J.A., KAUFMAN, Y., NAKAJIMA, T., LAVENU, F., JANKOWIAK, I. and SMIRNOV, A., 1998, AERONET—A federated instrument network and data archive for aerosol characterization. *Remote Sensing of Environment*, **66**, pp. 1–16.

KASISCHKE, E.S. and FRENCH, N.H.F., 1995, Locating and estimating the areal extent of wildfires in Alaskan boreal forests using multiple-season AVHRR NDVI composite data. *Remote Sensing of Environment*, **51**, pp. 263–275.

KNAPP, A.K. and SEASTEDT, T.R., 1986, Detritus accumulation limits productivity of tallgrass prairie. *BioScience*, **36**, pp. 662–668.

KRUGER, A.C., MAKAMO, L.B. and SHONGWE, S., 2002, An analysis of Skukuza climate data. *Koedoe*, **45**, pp. 1–7.

LANDMANN, T., 1999, A methodology to monitor fires in South African grasslands using Landsat Thematic Mapper satellite data. MSc thesis, Department of Landscape Ecology, University of Göttingen, Germany.

LANGAAS, S., 1995, Night-time observations of West-African bushfires from space: Studies on methods and applications of thermal NOAA/AVHRR satellite data from Senegal and the Gambia. PhD thesis, Department of Geography, University of Oslo, Norway.

LEMMON, P.E., 1957, A new instrument for measuring forest overstory density. *Journal of Forestry*, **55**, pp. 666–669.

LEVINE, J.S. (Ed.), 1996, *Biomass Burning and Global Change* (Cambridge, MA: MIT Press).

LOPEZ GARCIA, M.J. and CASELLES, V., 1991, Mapping burns and natural reforestation using Thematic Mapper data. *Geocarto International*, **1**, pp. 31–37.

MCDONALD, A.J., GEMMELL, F.M. and LEWIS, P.E., 1998, Investigation of the utility of spectral vegetation indices for determining information on coniferous forests. *Remote Sensing of Environment*, **66**, pp. 250–272.

MICHALEK, J.L., COLWELL, J.E., FRENCH, N.H.F., KASISCHKE, E.S. and JOHNSON, R.D., 2000, Using Landsat TM data to estimate carbon release from burned biomass in an Alaskan spruce forest complex. *International Journal of Remote Sensing*, **21**, pp. 329–343.

MILLER, J.D. and YOOL, S.R., 2002, Mapping post-fire canopy consumption in several overstory types using multi-temporal Landsat TM and ETM data. *Remote Sensing of Environment*, **82**, pp. 481–496.

NETSHILUVHI, T.R. and SCHOLES, R.J., 2001, Allometry of South African woodland trees. CSIR Environmentek ENV-P-I 2001-007. CSIR Division of Water, Environment and Forestry Technology, Pretoria, South Africa.

PEREIRA, J.M.C., 1999, A comparative evaluation of NOAA/AVHRR vegetation indexes for burned surface detection and mapping. *IEEE Transactions on Geoscience and Remote Sensing*, **37**, pp. 217–226.

REICHENBACH, S.E., KOEHLER, D.E. and STRELOW, D.W., 1995, Restoration and reconstruction of AVHRR images. *IEEE Transactions on Geoscience and Remote Sensing*, **33**, pp. 997–1007.

ROGAN, J. and YOOL, S.R., 2001, Mapping fire-induced vegetation depletion in the Peloncillo Mountains, Arizona and New Mexico. *International Journal of Remote Sensing*, **22**, pp. 3101–3121.

ROY, D.P., GIGLIO, L., KENDALL, J.D. and JUSTICE, C.O., 1999, Multi-temporal active-fire based scar detection algorithm. *International Journal of Remote Sensing*, **20**, pp. 1031–1038.

ROY, D.P., LEWIS, P.E. and JUSTICE, C.O., 2002, Burned area mapping using multi-temporal moderate spatial resolution data—a bi-directional reflectance model-based expectation approach. *Remote Sensing of Environment* (MODIS Land Special Issue), **83**, pp. 263–286.

SCHOLES, R.J., 1997, Savanna. In *Vegetation of Southern Africa*, R.M. Cowling, D.M. Richardson and S.M. Pierce (Eds), pp. 258–277 (Cambridge: Cambridge University Press).

SCHOLES, R.J., KENDALL, J. and JUSTICE, C.O., 1996, The quantity of biomass burned in southern Africa. *Journal of Geophysical Research*, **101**, pp. 23667–23676.

SCHULZE, R.E., 1997, Climate. In *Vegetation of Southern Africa*, R.M. Cowling, D.M. Richardson and S.M. Pierce (Eds), pp. 2–42 (Cambridge: Cambridge University Press).

SETTLE, J. and CAMPBELL, N., 1998, On the errors of two estimators of sub-pixel fractional cover when mixing is linear. *IEEE Transactions on Geoscience and Remote Sensing*, **36**, pp. 163–170.

SHEA, R.W., SHEA, B.W., KAUFFMAN, J.B., WARD, D.E., HASKINS, C.I. and SCHOLES, M., 1996, Fuel biomass and combustion factors associated with fires in savanna ecosystems of South Africa and Zambia. *Journal of Geophysical Research*, **101**, pp. 23551–23568.

STOCKS, B.J., VAN WILGEN, B.W., TROLLOPE, W.S.W., MCRAE, D.J., MASON, J.A., WEIRICH, F. and POTGIETER, A.L.F., 1996, Fuels and fire behavior dynamics on large-scale savanna fires in Kruger National Park, South Africa. *Journal of Geophysical Research*, **101**, pp. 23541–23550.

STRONACH, N.R.H. and MCNAUGHTON, S.J., 1989, Grassland fire dynamics in the Serengeti Ecosystem, and a potential method of retrospective estimating fire energy. *Journal of Applied Ecology*, **26**, pp. 1025–1033.

SWAP, R.J., ANNEGARN, H.J., SUTTLES, J.T., HAYWOOD, J., HELMLINGER, M.C., HELY, C., HOBBS, P.V., HOLBEN, B.N., JI, J., KING, M., LANDMANN, T., MAENHAUT, W., OTTER, L., PAK, B., PIKETH, S.J., PLATNICK, S., PRIVETTE, J., ROY, D.P., THOMPSON, A.M., WARD, D. and YOKELSON, R., 2002, The Southern African Regional Science Initiative (SAFARI 2000): overview of the dry-season field campaign. *South African Journal of Science*, **98**, pp. 125–130.

THOMPSON, M.W., 1993, *Quantitative Biomass Monitoring and Fire Severity Mapping Techniques in Savanna Environments Using Landsat Thematic Mapper Imagery*. External Contract Report FOR-DEA 587, Division of Water, Environment and Forest Technology, CSIR, Pretoria, South Africa.

TRIGG, S. and FLASSE, S., 2000, Characterizing the spectral-temporal response of burned savannah using *in situ* spectroradiometry and infrared thermometry. *International Journal of Remote Sensing*, **21**, pp. 3161–3168.

TROLLOPE, W.S.W. and TAINTON, N.M., 1986, Effect of fire intensity on the grass and bush componenets of the Eastern Cape Thornveld. *Journal of the Grassland Society of Southern Africa*, **2**, pp. 27–42.

TROLLOPE, W.S.W. and POTGIETER, A.L.F., 1986, Estimating grass fuel loads with a disc pasture meter in the Kruger National Park. *Journal of the Grassland Society of Southern Africa*, **3**, pp. 148–152.

VERMOTE, E.F., EL SALEOUS, N.Z. and JUSTICE, C.O., 2002, Atmospheric correction of the MODIS data in the visible to middle infrared: first results. *Remote Sensing of Environment* (MODIS Land Special Issue), **83**, pp. 97–111.

VERMOTE, E.F., TANRE, D., DEUZE, J.L., HERMAN, M. and MORCRETTE, J., 1997, Second simulation of the satellite signal in the solar spectrum, 6S: An overview. *IEEE Transaction on Geoscience and Remote Sensing*, **35**, pp. 675–686.

VERSTRAETE, M.M. and PINTY, B., 1996, Designing optimal spectral indexes for remote sensing applications. *IEEE Transactions on Geoscience and Remote Sensing*, **34**, pp. 1254–1265.

WARD, D.E., HAO, W.M., SUSOTT, R.A., BABBITT, R.E., SHEA, R.W., KAUFFMAN, J.B. and JUSTICE, C.O., 1996, Effect of fuel composition on combustion efficiency and emission factors for African savanna ecosystems. *Journal of Geophysical Research*, **101**, pp. 23569–23576.